Data driven approach in multiphysics framework: application to coupled electro-mechanical problems

Eduard Marenić, Guillem Seychal, Jean-Charles Passieux

Data driven approach in multiphysics framework: application to coupled electro-mechanical problems

Eduard Marenić[1,*], Guillem Seychal[1], and Jean-Charles Passieux[1]

[1] *Institut Clement Ader (ICA), Universit de Toulouse, CNRS-INSA-UPS-ISAE-Mines Albi, 135 avenue de Rangueil, 31077 Toulouse, France*
[*] *Corresponding author: Eduard Marenić, marenic@insa-toulouse.fr*

Abstract

Solving coupled multiphysics problems using finite elements and conventional modeling approach requires building, from coupled finite element formulation often in the same code, the monophysical operators and the multiphysics coupling operators. In this work the data driven, model-free computational approach is fitted in the multiphysics framework adapted for 'smart' materials. Thus, in this work we ought to expand the phase space and propose a new norm for the distance based data driven solver adapted to the problem at hands. Given the good material database which naturally encodes the coupling interactions, we show that proposed application of data driven approach enables to avoid the coupling tangent terms altogether. In other words, the data driven approach permits to decouple the different 'physics' and to manage the coupling from the data. We illustrate the performance and robustness of the approach on two examples related to lattice model composed of planar, piezoelectric truss network and of finite element discretized linear piezoelectric solids. The numerical tests show a good convergence properties related to the number of data points, as well as the choice of material and weighting parameters.

Keywords— Data driven approach, model-free, data driven computational mechanics, multiphysics, coupled problem, piezoelectricity.

1 Introduction

Typical problem in computational mechanics considers the response of a solid deformable body under applied loading, leading to the boundary value problem (BVP). In this context one's main interest is to compute three fields, namely, displacements, strains and stresses, which have to be in agreement with prescribed mechanical properties, applied external loading and the conditions imposed on the boundary. The governing equations of the typical BVP are defined with

(i) kinematics equations, (ii) equilibrium equations, and (iii) constitutive equations. While (i) and (ii) are related to geometry and conservation laws, one of the fundamental issues that scientists and engineers are confronted with is the characterization of the mechanical behaviour of material, given with (iii).
The classic approach in the computational mechanics considers the formulation of material models whose development relies on the *data* usually collected through 'testing'. A modern test (performed mostly in the design and development phase) of engineering product concerns (a) real instrumented experiments with a variety of sensors and setups, and (b) virtual experiments, simulations using different models and numerical methods. Both (a) and (b) are performed on different scales ranging from material to structural scale. In the 1960s the available data were sparse across certain regimes and were gathered through poorly instrumented experiments (a) using extensometry, strain gauges and force cells. These experiments were complemented with analytical or rather simple numerical methods. Thus, one needed a great deal of intuition and experience to develop a quality model from usually scarce input with the purpose of generalizing experimental measurements mostly performed on simple tests. This situation has changed: the models became more complex together with the significant development of dedicated numerical methods. Accordingly, instrumented experiments (a) lean to full-field kinematic/thermal measurements [1] giving rise to so-called data assimilation. That is, the transition to the data rich era progressively happened in computational mechanics. On the other hand, traditional models were developed in a different context which sometimes makes them incompatible with the data rich environment, finally causing the model with it's assumed properties to downgrade the available data. In other words, traditional fitting of a model to the 'big data' is often ill-posed and can cause modeling errors which might severely impact the accuracy of the solution.
Data driven computational mechanics (DDCM) [2] is a generalization of traditional, modeling approach in computational mechanics. More precisely, DDCM is a reformulation of BVP aiming to search for the solution in the set of mechanically admissible states by minimizing the distance to the material data set (a point set). The basic idea behind DDCM is to use the provided measurements (coming from tests (a) or (b)) as constitutive data directly in the computation, skipping entirely the modeling step and the usage of the constitutive model. In the narrow sense, a mechanically admissible state is a tuple (strain, stress) which satisfies (i) kinematic and (ii) equilibrium relations, as well as the related boundary conditions. In this context, the data driven problem is defined with double minimization of the squared distance in the phase space and the objective is to find an admissible state the closest to the material state, also given with the tuple (strain, stress). So called distance-based solver is introduced in [2] to solve data driven problem, *i.e.*, to iteratively minimize the distance between admissible and material states. In each iteration within a staggered solution scheme we are: 1) projecting the material state to an admissible set which boils down to solving two linear systems resulting from finite element discretization, and 2) searching the closest point in data set to the previously calculated point in admissible set. Note that linearity of two linear systems

solved in step 1) is completely independent of the linearity or non-linearity of the material behavior. We note also, that in the frame of data driven approach (DDA) the spatial (and temporal) discretization(s) are still kept the same as in the classic approach and are mostly related to finite element method.
From it's introduction the performance of the DDCM as the new 'model-free' computational paradigm was presented in static [2, 3] and dynamic [4] context. The convergence analysis of the proposed solver is presented for the linear [2, 3] and non-linear [5, 6] elastic behavior. In the last five years the model-free approach is emerging as an alternative to model-based computing and was extended to inelasticity [7], fracture [8] and multiscale problems [9, 10]. We also note the work related to data driven identification (DDI) introduced by Leygue [11, 12], permitting to identify stress from mechanical tests and digital image correlation. The idea of DDI is to identify the stresses from full-field measurements without *a priori* knowledge of material model, see [13]. To the author's knowledge there were no attempts to extend the model-free approach to coupled, multiphysics problems addressed in the sequel.

Modern consumer electronics has pushed the boundaries of technological development towards miniaturization with weight/size limitations and power demands being the two most stringent requirements. Smart (active) materials fit nicely to those strict requirements and many of them are nowadays used in various fields of engineering and modern technologies [14, 15]. The 'smartness' of these materials relies on their transducer capabilities (actuation/sensing), that is, the capability to receive, transmit, or process a stimulus and respond by producing a useful effect. The receiving/responding capability of the smart material is achieved by converting energy between different physical fields, for instance: mechanical, thermal, electric and magnetic [16, 17, 18, 19]. In the multi-field context one needs to take care, firstly, of so-called *principal interactions* which govern the relation between work conjugate variables for each physical field. Secondly, since smart materials rely on the significant coupling between different physical fields, one needs to take care of *coupled interactions*. These interactions are for magneto-electro-. . .-elastic solids governed by constitutive relations (iii). In the multiphysics context, the constitutive relations are formulated in an energy framework through thermodynamic potentials, see [18]. According to [18] eight different forms of constitutive relations can be developed depending on the choice of independent variables. Regardless of the choice of independent variables, the state is in the multi-coupled framework defined by N-tuple, where $N = 2n$ is the number of state variables and n is the number of coupled fields. For the four-field example ($n = 4$) mentioned above we have 8-tuples (strain $\boldsymbol{\sigma}$, stress $\boldsymbol{\varepsilon}$; electric field $\mathbf{E}$, polarization $\mathbf{D}$; magnetic field $\mathbf{H}$, magnetization $\mathbf{M}$; temperature T, entropy S). The relation between state variables (choosing for instance $\boldsymbol{\varepsilon}, \mathbf{E}, \mathbf{H}, T$ as independent) for the reversible

processes [17] can be given as

$$\begin{bmatrix} \mathrm{d}\boldsymbol{\sigma} \\ \mathrm{d}\mathbf{D} \\ \mathrm{d}\mathbf{M} \\ \mathrm{d}S \end{bmatrix} = \begin{bmatrix} \frac{\partial \boldsymbol{\sigma}}{\partial \boldsymbol{\varepsilon}} & \frac{\partial \boldsymbol{\sigma}}{\partial \mathbf{E}} & \frac{\partial \boldsymbol{\sigma}}{\partial \mathbf{H}} & \frac{\partial \boldsymbol{\sigma}}{\partial T} \\ \frac{\partial \mathbf{D}}{\partial \boldsymbol{\varepsilon}} & \frac{\partial \mathbf{D}}{\partial \mathbf{E}} & \frac{\partial \mathbf{D}}{\partial \mathbf{H}} & \frac{\partial \mathbf{D}}{\partial T} \\ \frac{\partial \mathbf{M}}{\partial \boldsymbol{\varepsilon}} & \frac{\partial \mathbf{M}}{\partial \mathbf{E}} & \frac{\partial \mathbf{M}}{\partial \mathbf{H}} & \frac{\partial \mathbf{M}}{\partial T} \\ \frac{\partial S}{\partial \boldsymbol{\varepsilon}} & \frac{\partial S}{\partial \mathbf{E}} & \frac{\partial S}{\partial \mathbf{H}} & \frac{\partial S}{\partial T} \end{bmatrix} \begin{bmatrix} \mathrm{d}\boldsymbol{\varepsilon} \\ \mathrm{d}\mathbf{E} \\ \mathrm{d}\mathbf{H} \\ \mathrm{d}T \end{bmatrix}. \tag{1}$$

The constitutive relations in the four-field context gather all the principal interaction given on the diagonal of the constitutive matrix in (1), that is, elasticity between strain-stress, electric susceptibility[1] for electric field-polarization, magnetic susceptibility for magnetic field-magnetization and heat capacity relating temperature to entropy. Off-diagonal terms in (1) represent the coupled properties giving rise to well known effects like piezoelectricity related to electro-mechanical coupling, magnetostriction related to magneto-mechanical coupling, pyroelectricity related to coupling between heat and electric field, etc. These coupled interactions are expressed as tensors gathering all the magnetoelectric, piezoelectric, piezomagnetic, thermoelastic, and thermoelectric constants (both for direct and inverse effects).
Lastly, we note that the finite element (FE) formulation of the coupled problem requires the assembly of a number of residual and tangent operators. The latter are in the coupled context largely expanded, that is, in the four-field coupled context we obtain by linearizing the mechanical residual (see section 5.2.3 in [17]) the direct mechanical stiffness (relating forces and displacements) but also three coupling tangent operators relating displacements with other degrees of freedom as for instance electrical and magnetic potentials and temperature. Analogously, linearizing other residuals gives other direct and coupled tangent operators. Clearly, the assembly of the FE operators that encode the coupling scales with $n(n-1)/2$ and will lead to increased computational cost in the multi-coupled problems. In addition, a classic, model-based FE solution requires a considerable number of material parameters to be measured and an adequate model (the one governing all the principal and coupled interactions) which implicitly directs the measuring procedure of the parameters.

The objective of the proposed work is to pave the way for data-driven computing in the frame of coupled, multiphysics problems in solid mechanics. In this work as a first step, we propose to extend the method of DDCM to a two-field example of the coupled electro-mechanical interaction. In this context, we focus on the common active materials in the form of piezoelectric solids [20, 15] featuring a direct and inverse piezoelectric effect to exchange the energy between mechanical and dielectric fields. More precisely, we will deal with ferroelectric materials featuring a domain structure which permits a remanent polarization.

[1] In sequel of this paper we will use the electric permittivity and electrical displacement directly knowing the relations between polarization and electrical displacement as well as between susceptibility and relative permittivity.

In the presented examples we focus primarily on the lead zirconate titanate (PZT), which is the most common ferroelectric material used for piezoelectric actuators and sensors. From it's development piezoelectric transducers found it's application in many fields [21] which was followed by an effort in the development of the FE modeling using continuum, and structural finite elements [22, 23, 24, 25, 26].

To that end, we give in the next section a brief review of the piezoelectric model and related governing equations as well as the FE formulation of the coupled electro-mechanical problem. In section 3 the application of the model-free approach to the electro-mechanical problem at hands is detailed. The convergence and the robustness of the data driven algorithm for coupled material response is firstly presented on the simple example of the piezoelectric lattice structure comprising a number of 1D bars and then generalized to 2D problems in the section 4. In the last section, a conclusion and a perspective for future work is discussed.

2 Governing equations of the piezoelectric model

For completeness in this section we briefly revisit the BVP of the piezoelectric continua, having the same general structure and properties, namely kinematic (i), equilibirum (ii) and constitutive (iii) relations, as the standard, mechanical BVP. The difference is that the governing equations are related to 1. mechanical (M) sub-problem described by elastostatics / elastodynamics, related kinematics and boundary conditions; 2. electrical (E) sub-problem related to the electrostatics Gauss, Maxwell law and related boundary conditions; 3. coupling which manifests itself only through the constitutive relations. All the quantities appearing in the model are summarized in Table 1. The number of indices in Table 1 describes the order of the tensor ranging, in the presented model, from scalar to 4^{th} order tensor. For simplicity of notation index notation is in sequel abandoned in favor of the symbolic, denoting all the vectors and tensors in bold. We focus in sequel on the piezoelectric body occupying a bounded domain

		(M)			(E)
u_i	$[\mathrm{m}]$	displacement vector	φ	$[\mathrm{V}=\frac{\mathrm{J}}{\mathrm{C}}]$	electric potential
b_i	$[\frac{\mathrm{N}}{\mathrm{m}^3}]$	body force vector	ρ_q^v	$[\frac{\mathrm{C}}{\mathrm{m}^3}]$	electric body charge
ε_{ij}	$[\frac{\mathrm{m}}{\mathrm{m}}]$	strain tensor	E_i	$[\frac{\mathrm{V}}{\mathrm{m}}=\frac{\mathrm{N}}{\mathrm{C}}]$	electric field vector
σ_{ij}	$[\frac{\mathrm{N}}{\mathrm{m}^2}]$	stress tensor	D_i	$[\frac{\mathrm{C}}{\mathrm{m}^2}]$	el. displacement vector
C_{ijkl}	$[\frac{\mathrm{N}}{\mathrm{m}^2}]$	stiffness tensor	ϵ_{ij}	$[\frac{\mathrm{F}}{\mathrm{m}}=\frac{\mathrm{C}}{\mathrm{Vm}}]$	el. permittivity tensor
S_{ijkl}	$[\frac{\mathrm{m}^2}{\mathrm{N}}]$	compliance tensor	ϵ_{ij}^{-1}	$[\frac{\mathrm{m}}{\mathrm{F}}]$	inverse of el. permit.
	(M)(E)	e_{kij}	$[\frac{\mathrm{C}}{\mathrm{m}^2}=\frac{\mathrm{N}}{\mathrm{Vm}}]$	piezoelectric (stress) constants tensor	
	(M)(E)	d_{kij}	$[\frac{\mathrm{C}}{\mathrm{N}}=\frac{\mathrm{m}}{\mathrm{V}}]$	piezoelectric (strain) constants tensor	

Table 1: Quantities used in the piezoelectric model with corresponding units in SI system, where (M) denotes mechanical and (E) electrical quantities.

$\Omega \subset \mathbb{R}^3$ with the boundary Γ, see Fig. 1.

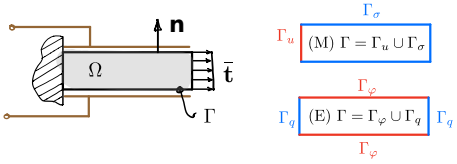

Figure 1: A piezoelectric slab of volume Ω with the boundary Γ. The boundary Γ is split to Dirichlet and Neumann parts in both mechanical and electrical problems: (M) the body is encastred on the left and loaded on the right while the upper and lower surfaces are traction-free; (E) the electrodes are attached to the upper and lower surfaces permitting to fix the electric potential, while the surfaces on the right and left have the charge imposed.

Boundary conditions The boundary Γ is partitioned to mechanical and electrical parts as : (M) $\Gamma = \Gamma_u \cup \Gamma_\sigma$, and (E) $\Gamma = \Gamma_\varphi \cup \Gamma_q$, see Fig. 1 (right), with $\Gamma_u \cap \Gamma_\sigma = \emptyset$ and $\Gamma_\phi \cap \Gamma_q = \emptyset$ to ensure well-posedness of the BVP. It should be noted that the boundary conditions (BC) in piezoelectricity are uncoupled, that is, the standard mechanical conditions are applied separately from the electrical boundary conditions. Moreover, the partition of the boundary into disjunctive parts (related to Dirichlet and Neumann parts) can be done completely independently for mechanical and electrical sub-problems. Thus, the parts: (M) Γ_u and Γ_σ respectively support a prescribed displacement $\bar{\mathbf{u}}$ and prescribed traction $\bar{\mathbf{t}}$; while (E) Γ_φ and Γ_q respectively support a prescribed electric potential $\bar{\varphi}$ and a prescribed surface charge density $\bar{q}$.

Kinematics (i) The kinematics relations for mechanical part (M) define the strain tensor (we limit our study to small displacement gradients), while the dielectric equivalent (E) is given through the Maxwell's law defining the electric field vector $\mathbf{E}$ as the negative gradient of electric potential:

$$(M): \quad \boldsymbol{\varepsilon} = \frac{1}{2}(\operatorname{grad}\mathbf{u} + \operatorname{grad}\mathbf{u}^{\mathrm{T}}), \qquad (E): \quad \mathbf{E} = -\operatorname{grad}\varphi. \tag{2}$$

Associated BC are given as

$$(M): \quad \mathbf{u} = \bar{\mathbf{u}} \quad \text{on } \Gamma_u, \qquad (E): \quad \varphi = \bar{\varphi} \quad \text{on } \Gamma_\varphi. \tag{3}$$

Equilibrium (ii) The local mechanical equilibrium (M) has it's dielectric equivalent in terms of the Gauss law. That is, for any point in Ω we have

$$(M): \quad \operatorname{div}\boldsymbol{\sigma} + \mathbf{b} = \mathbf{0}, \qquad (E): \quad \operatorname{div}\mathbf{D} = \rho_q^v = 0. \tag{4}$$

Related BC with imposed quantities $\bar{\mathbf{t}}, \bar{q}$ can be given as

$$(M): \quad \boldsymbol{\sigma}\,\mathbf{n} = \bar{\mathbf{t}} \quad \text{on } \Gamma_\sigma, \qquad (E): \quad \mathbf{D}\,\mathbf{n} = -\bar{q} \quad \text{on } \Gamma_q. \tag{5}$$

where $\mathbf{n}$ represents the outward unit normal on Γ, and $\bar{\mathbf{t}}, \bar{q}$ the imposed quantities.

Constitutive relations (iii) - to be replaced with data By extracting the first two lines and columns from the general form given in (1) we can obtain the piezoelectric constitutive relations. We note also (proof omitted) that the off-diagonal, coupled properties in the extracted 2x2 matrix are equal $\frac{\partial \boldsymbol{\sigma}}{\partial \mathbf{E}} = \frac{\partial \mathbf{D}}{\partial \boldsymbol{\varepsilon}} = \mathbf{e}^\top$, that is, the direct and converse piezoelectric effects are equivalent. Integrating the subsystem related to electro-mechanical coupling we obtain the constitutive relations of the linear piezoelectricity (in the so called stress form[2] with independent variables $(\boldsymbol{\varepsilon}, \mathbf{E})$:

$$\begin{aligned} \boldsymbol{\sigma} &= \mathbf{C}_{|_E}\, \boldsymbol{\varepsilon} - \mathbf{e}^\top\, \mathbf{E}, \\ \mathbf{D} &= \mathbf{e}\, \boldsymbol{\varepsilon} + \boldsymbol{\epsilon}_{|_\varepsilon}\, \mathbf{E}. \end{aligned} \tag{6}$$

The above relations are coupling linear elasticity (with Hooke's stiffness operator $\mathbf{C}$) to the charge equation of electrostatics (with permittivity matrix $\boldsymbol{\epsilon}$) using piezoelectric constants stored in $\mathbf{e}$. We note that this group of equations is going to be replaced with data in sequel within DDA.

Weak form and classic finite element (FE) formulation Before closing this section we give a brief overview of the numerical solution of the presented BVP in piezoelectricity and, following the usual practice, we abandon the strong form in favor of the weak form of equilibrium (ii). On top of elasticity where we weaken the equilibrium equation, we ought to weaken the conditions of the Gauss law. Choosing kinematically admissible virtual displacement field $\mathbf{u}^\star$ and virtual electric potential $\varphi^\star$, such that both fields are regular and $\mathbf{u}^\star = \mathbf{0}$ on Γ_u, and $\varphi^\star = 0$ on Γ_φ we have

$$\forall \mathbf{u}^\star, \qquad \int_\Omega \mathbf{u}^\star \operatorname{div} \boldsymbol{\sigma}\, d\Omega = 0 = \int_\Gamma \mathbf{u}^\star \boldsymbol{\sigma}\, \mathbf{n}\, d\Gamma - \int_\Omega \operatorname{grad} \mathbf{u}^\star \boldsymbol{\sigma}\, d\Omega, \tag{7}$$

$$\forall \varphi^\star, \qquad \int_\Omega \varphi^\star \operatorname{div} \mathbf{D}\, d\Omega = 0 = \int_\Gamma \varphi^\star \mathbf{D}\, \mathbf{n}\, d\Gamma - \int_\Omega \operatorname{grad} \varphi^\star \mathbf{D}\, d\Omega. \tag{8}$$

FE formulation resides on the standard continuum FEs, see *e.g.* [22], adding for piezoelectric materials, the degree of freedom related to electric potential (φ) in each node.

Remark. *Standard FE solution of the coupled problem (here the piezoelectric BVP) requires a custom-made FEs with added degrees of freedom. Since general, multi-coupled formulation (e.g. four-field example from the Introduction, [17]) is rarely a part of the standard codes used in computational mechanics, one*

[2] We are free to choose independent variables in the formulation of the constitutive law. For many applications, different choices of independent variables may fit better. Strain form with independent variables $(\boldsymbol{\sigma}, \mathbf{E})$ gives rise to coupling operator $\mathbf{d}$ shown in Table 1.

needs to have an access to the code source or master user element routines. We show in the sequel that DDA approach makes the electro-mechanical coupling non-invasive (see [27]).

The discrete system arising from FE discretization consists of N_n nodes and N_i integration (material) points. The spacial interpolation of displacement and electric potential fields can be given using standard FE shape functions stored in $\mathbf{N}$

$$\mathbf{u}(\mathbf{x}) = \mathbf{N}^M \mathbf{u}_n \qquad \text{and} \qquad \varphi(\mathbf{x}) = \mathbf{N}^E \boldsymbol{\varphi}. \tag{9}$$

Having the displacement and potential fields and related interpolation in hands, using (2), we can express the strain and electric field in each material point i as

$$\boldsymbol{\varepsilon}_i = \mathbf{B}_i^M \mathbf{u} \qquad \text{and} \qquad \mathbf{E}_i = \mathbf{B}_i^E \boldsymbol{\varphi}, \tag{10}$$

where $\mathbf{B}_i^M$ is standard strain operator (symmetric gradient of FE shape functions) for integration point i, while $\mathbf{B}_i^E$ is simply the gradient of FE shape functions. Performing analogous procedure for the virtual fields $(\mathbf{u}^\star, \varphi^\star)$, plugging these interpolations into weak form (7), (8) and taking into account BC (3), (5) we finally have

$$\sum_i^{N_i} w_i \mathbf{B}_i^{M,\top} \boldsymbol{\sigma}_i = \mathbf{f} \qquad \text{and} \qquad \sum_i^{N_i} w_i \mathbf{B}_i^{E,\top} \mathbf{D}_i = \mathbf{f}^q, \tag{11}$$

where w_i denotes integration weights, while active nodal forces vector $\mathbf{f}$ and nodal charges vector in $\mathbf{f}^q$ read:

$$\mathbf{f} = \int_{\Gamma_\sigma} \mathbf{N}^{M\top} \bar{\mathbf{t}} \, d\Gamma \qquad \text{and} \qquad \mathbf{f}^q = \int_{\Gamma_q} \mathbf{N}^{E\top} \bar{q} \, d\Gamma. \tag{12}$$

Moreover, by including the constitutive equations (6) we end up (details in *e.g.* [22]) with the linear system

$$\begin{bmatrix} \mathbf{K}^M & \mathbf{K}^{EM} \\ \mathbf{K}^{EM,\top} & \mathbf{K}^E \end{bmatrix} \begin{bmatrix} \mathbf{u} \\ \boldsymbol{\varphi} \end{bmatrix} = \begin{bmatrix} \mathbf{f} \\ -\mathbf{f}^q \end{bmatrix}, \tag{13}$$

where $\mathbf{K}^M$ and $\mathbf{K}^E$ are the stiffness matrix and the dielectric 'stiffness' matrix, while $\mathbf{K}^{EM}$ is the piezoelectric 'stiffness' matrix governing the coupling.

Remark. *Related to the previous remark, we note here that the classic FEM solution resides on the coupling model encoded in the coupling stiffness-like operator $\mathbf{K}^{EM}$ which needs to be assembled requiring, thus, a specific multiphysics code.*

The benefit of the DDA extended to fit in the multiphysics context is twofold since in addition to skipping the material (inhere) coupling model, we aim to completely decouple the problem. More precisely the DDA will permit a numerical implementation which doesn't take care of the coupling.

3 Data driven approach for coupled electro-mechanical problem

In this section DDA originally developed for elasticity (see [2] and references cited in the Introduction) is applied to the coupled electro-mechanical problem at hands. This development relies on three points: a) expansion of the phase space, b) redefinition of the norm to metrize the new phase space and c) reformulation of the DDA problem.

As opposed to 'standard' DDA related to elasticity where the local state of the system in every point i is characterized by solely the stress and strain pairs, here we ought to expand the phase space. That is, for the two-field[3] case we describe the state with quadruples $(\boldsymbol{\varepsilon}_i, \boldsymbol{\sigma}_i; \mathbf{E}_i, \mathbf{D}_i)$ with: $(\boldsymbol{\varepsilon}_i, \boldsymbol{\sigma}_i) \in \mathbb{R}^{d_M}$ and $(\mathbf{E}_i, \mathbf{D}_i) \in \mathbb{R}^{d_E}$, where d_M, and d_E are the dimensions of stress and strain, and electrical field and displacement, respectively, at each point i. We denote, thus, $\mathbf{z}_i = (\boldsymbol{\varepsilon}_i, \boldsymbol{\sigma}_i; \mathbf{E}_i, \mathbf{D}_i)$ a point in a phase space $Z = \mathbb{R}^{2d_M} \times \mathbb{R}^{2d_E}$. The internal states $\mathbf{z} = [(\boldsymbol{\varepsilon}_i, \boldsymbol{\sigma}_i; \mathbf{E}_i, \mathbf{D}_i)]_{i=1}^{N_i}$ which exactly satisfy the kinematics (10) and equilibrium (11) are considered as the electro-mechanical states. In the classic, modeling approach the set of equations (2) and (4) is closed with the continuous relation between state variables expressed for instance in (6). The main novelty of DDA, as discussed in the Introduction, is to avoid entirely the usage of the material model in favor of the material database[4]. To that end, the modeling approach is reformulated and in addition to being compatible (i) and equilibrated (ii), the electro-mechanical state has to be close to the material response stored in the database, and not any more verify the constitutive law (iii). In other words, we tend to assign to each electro-mechanical state $\mathbf{z}_i$ closest material state from the database. The latter is in our context composed of material data points $\mathbf{z}_m = (\boldsymbol{\epsilon}_m, \boldsymbol{\sigma}_m; \mathbf{E}_m, \mathbf{D}_m) \in Z$, where $m = 1 \dots N_m$, and N_m denotes the number of the material points in the database. We denote the material state $\mathbf{z}_m$ assigned to the electro-mechanical state $\mathbf{z}_i$ as $\mathbf{z}_{im}$, where im denotes the pairing.

In order to metrize the distance in the extended phase space the following electro-mechanical norm is proposed:

$$\|\mathbf{z}_i\|_{EM}^2 = \alpha(\boldsymbol{\varepsilon}_i^\top \mathbf{C} \boldsymbol{\varepsilon}_i + \boldsymbol{\sigma}_i^\top \mathbf{C}^{-1} \boldsymbol{\sigma}_i) + (1-\alpha)(\mathbf{E}_i^\top \boldsymbol{\epsilon} \mathbf{E}_i + \mathbf{D}_i^\top \boldsymbol{\epsilon}^{-1} \mathbf{D}_i), \qquad (14)$$

where synthetic operators $\mathbf{C}$ and $\boldsymbol{\epsilon}$ gather numerical constants rather then the ones related to the real material with the goal to weight the influence from the work-conjugate pairs $(\boldsymbol{\varepsilon} - \boldsymbol{\sigma}, \mathbf{E} - \mathbf{D})$; α is used to weight the influence of the two terms on the right-hand side related to (M) and (E) contribution. With this norm in hands we can express the squared distance between electro-mechanical

[3] The two-field example, which is the focus of this paper, is a particular case of the general multiphysics context discussed in the Introduction. We denote, thus, the two-fields case with $n = 2$ for elasticity and electricity, and the electro-mechanical states which are defined with quadruples, $N = 2n = 4$.

[4] Recall that the points in the database are obtained by 'tests', either real (a) or virtual (b) (see Introduction).

state and associated data point as

$$d_i^2 = \|\mathbf{z}_i - \mathbf{z}_{im}\|_{EM}^2 \,. \tag{15}$$

With the proposed expansion of the phase space and the redefinition of the norm, the central problem of DDA for the case of piezoelectric continua is formally written as:
Given: FE mesh (geometry and connectivity), boundary conditions and material database $\mathbf{z}_m, m = 1 \dots N_m$,
Find: electro-mechanical states $\mathbf{z}_i$ and their pairing im with corresponding closest material states, such that it minimizes the global distance

$$\frac{1}{2}\left(\sum_i^{N_i} w_i \|\mathbf{z}_i - \mathbf{z}_{im}\|_{EM}^2\right)^{1/2}, \tag{16}$$

under constraints (10) and (11).
Clearly, the extended DDA problem still represents a constrained minimization problem with continuous and discrete variables as in standard DDA. Thus, we are going to reuse the same staggered solution scheme proposed in the original paper [2] with characteristic two steps in a single iteration:

1. Standard constrained minimisation problem for a given material pairing im in each point i. The pairing is known from initialization or previous iteration and stored to im.

2. Finding the closest material point for the known electro-mechanical state (pairing update).

As suggested in [2] in this work the initialisation of the pairing given with (im) relies simply on the random choice of data points paired to each material/integration point. In the original work Kirchdoerfer and Ortiz demonstrated insensitivity of the staggered solution scheme to such initialization, see Fig. 6 in [2]. The details of the reformulation of the distance-minimizing algorithm are given in the sequel.

DDA algorithm We start by plugging constraints in the minimisation problem. The kinematic constraint (10) is imposed directly, while the equilibrium (11) is enforced using Lagrange multipliers method which gives a functional $L = L^M + L^E$, for mechanical (M) and electrical (E) parts

$$L^M = \sum_i^{N_m}\left(\frac{w_i\mathbf{C}}{2}(\mathbf{B}_i^M\mathbf{u} - \boldsymbol{\varepsilon}_{im})^2 + \frac{w_i\mathbf{C}^{-1}}{2}(\boldsymbol{\sigma}_i - \boldsymbol{\sigma}_{im})^2 - (w_i\mathbf{B}_i^M\boldsymbol{\sigma}_i - \mathbf{f})\boldsymbol{\eta}\right), \tag{17}$$

$$L^E = \sum_i^{N_m}\left(\frac{w_i\boldsymbol{\epsilon}}{2}(\mathbf{B}_i^E\boldsymbol{\varphi} - E_{im})^2 + \frac{w_i\boldsymbol{\epsilon}^{-1}}{2}(\mathbf{D}_i - \mathbf{D}_{im})^2 - (w_i\mathbf{B}_i^E E_i - \mathbf{f}^q)\boldsymbol{\zeta}\right), \tag{18}$$

where multipliers $\boldsymbol{\eta}$ and $\boldsymbol{\zeta}$ represent virtual displacement and electric potential vectors, respectively. The minimisation of L with respect to $\mathbf{u}, \boldsymbol{\sigma}_i$ and $\boldsymbol{\eta}$ for the former, and with respect to $\boldsymbol{\varphi}, \mathbf{D}_i$ and $\boldsymbol{\zeta}$ for the latter leads to four linear systems (details omitted)

$$\begin{aligned}\left(\sum_i^{N_m} w_i \mathbf{B}_i^{M,\top} \mathbf{C}\, \mathbf{B}_i^M\right) \mathbf{u} &= \sum_i^{N_m} w_i \mathbf{B}_i^{M,\top} \mathbf{C} \boldsymbol{\varepsilon}_{im}, \\ \left(\sum_i^{N_m} w_i \mathbf{B}_i^{M,\top} \mathbf{C}\, \mathbf{B}_i^M\right) \boldsymbol{\eta} &= \mathbf{f} - \sum_i^{N_m} w_i \mathbf{B}_i^{M,\top} \boldsymbol{\sigma}_{im}.\end{aligned} \tag{19}$$

$$\begin{aligned}\left(\sum_i^{N_m} w_i \mathbf{B}_i^{E,\top} \boldsymbol{\epsilon}\, \mathbf{B}_i^E\right) \boldsymbol{\varphi} &= \sum_i^{N_m} w_i \mathbf{B}_i^{E,\top} \boldsymbol{\epsilon} \mathbf{E}_{im}, \\ \left(\sum_i^{N_m} w_i \mathbf{B}_i^{E,\top} \boldsymbol{\epsilon}\, \mathbf{B}_i^E\right) \boldsymbol{\zeta} &= \mathbf{f}^q - \sum_i^{N_m} w_i \mathbf{B}_i^{E,\top} \mathbf{D}_{im}.\end{aligned} \tag{20}$$

Two systems in (19) featuring operator $\mathbf{K}^M$ on the left-hand side are the standard product of DDA in elasticity. These systems have a standard form governing the displacements $(\mathbf{u}, \boldsymbol{\eta})$ generated by the forces associated to the quasi-stiffness ('quasi' in the sense of numerical, non-material parameters in $\mathbf{C}$). On the other hand, the systems in (20) featuring $\mathbf{K}^E$ on the left-hand side are added due to proposed application to the coupled problems. By analogy, a standard form is kept governing the electric potentials $(\boldsymbol{\varphi}, \boldsymbol{\zeta})$ generated by the generalized forces associated to the quasi-stiffness (featuring numerical, non-material parameters in $\boldsymbol{\epsilon}$).

Remark. *We note that the DDA approach turns the coupled problem (here a two-field coupling) which is in the classic, modeling approach governed by the system* (13) *into uncoupled. That is, in the equations above the coupling operator* $\mathbf{K}^{EM}$ *doesn't appear and the coupling is completely encoded in the material database.*

Solving the four systems for $\mathbf{u}, \boldsymbol{\eta}, \boldsymbol{\varphi}, \boldsymbol{\zeta}$ is the hidden step within the DDA algorithm and the true result is the post-processed electro-mechanical state $(\boldsymbol{\epsilon}_i, \boldsymbol{\sigma}_i; \mathbf{E}_i, \mathbf{D}_i), \forall i$ obtained by means of:

1. relation (10) and $\mathbf{u}, \boldsymbol{\varphi}$ to compute $\boldsymbol{\varepsilon}_i, \mathbf{E}_i$, and
2. $\boldsymbol{\eta}, \boldsymbol{\zeta}$ and the optimality conditions of $\nabla L = 0$ with respect to $\boldsymbol{\sigma}_i$ and $\mathbf{D}_i$ yielding

$$\boldsymbol{\sigma}_i = \boldsymbol{\sigma}_{im} + \mathbf{C}\, \mathbf{B}^M \boldsymbol{\eta}, \qquad \mathbf{D}_i = \mathbf{D}_{im} + \boldsymbol{\epsilon}\, \mathbf{B}^E \boldsymbol{\zeta}. \tag{21}$$

This solution represents a projection of the given material state (known pairing im for each i) to the electro-mechanical state respecting the kinematical and

equilibrium constraints.
In the second step of the single iteration within proposed algorithm we take the newly found electro-mechanical state and seek to reassign the material states for each point i such that

$$im = \arg\min_{m} \|\mathbf{z}_i - \mathbf{z}_m\|^2_{EM} \,. \tag{22}$$

This step can be seen as a projection of the electro-material states to the material database. Both of these projections are performed with the help of electro-mechanical norm (14).
This characteristic two-step iteration is repeated within distance-based solver until convergence. While the initialisation is often simply a random choice of pairings (im), the convergence considers that no closer material points can be found. The implementation and performance of the proposed reformulation of DDA is shown in the next section.

4 Numerical examples

4.1 Piezoelectric truss in lattice model

We consider in this section a lattice model [28] composed of planar truss network [29]. Contrarily to the standard FE discretization, in presented lattice model the domain is represented by the Voronoi tessellation with random geometry, as shown in the upper subplot on the Fig. 2 (a). In this case a planar truss network is forming the Delaunay triangulation, the dual of the Voronoi diagram, see the lower subplot on the Fig. 2 (a). Trusses in lattice model represent the cohesive links (t_{pk}) which hold the particles p and k together, see Fig. 2 (a). A zoom on those two particles p and k is given on the Fig. 2 (b) showing the characteristic height of the cross-section h_{pk} of the truss t_{pk} which is extracted from the underlying Voronoi tessellation. An overlap of the truss network (Delaunay) holding particles (Voronoi) together constructed on the rectangular domain 100×100 mm^2 is depicted on the Fig. 2 (c). We note in passing that the lattice modeling described above is usually applied to the inelastic and failure behavior of quasi-brittle materials. To that end the truss network described above is often replaced by beams or so-called rigid-body springs [30, 31] to properly describe shear failure modes.
Herein, we focus on the linear coupled elasto-dielectric behaviour, and we fit it in the context of the lattice modeling. For simplicity we are neglecting the time dependent features of inelastic response with the goal of testing the proposed application of DDA to the coupled problem. To that end, we consider lattice electroded on the upper and lower surfaces as depicted on Fig. 2 (c). This lattice represents a truss network composed of bi-articulated, cylindrical bars (t_{pk}). Each bar has the cross-section defined by the geometry (h_{pk}) of the shared edge of the two Voronoi cells and is polarized in the axial direction of the bar. The lateral surface of each bar is traction-free and without electrodes, while the end surfaces can be electroded and under uniform traction/compression leading to

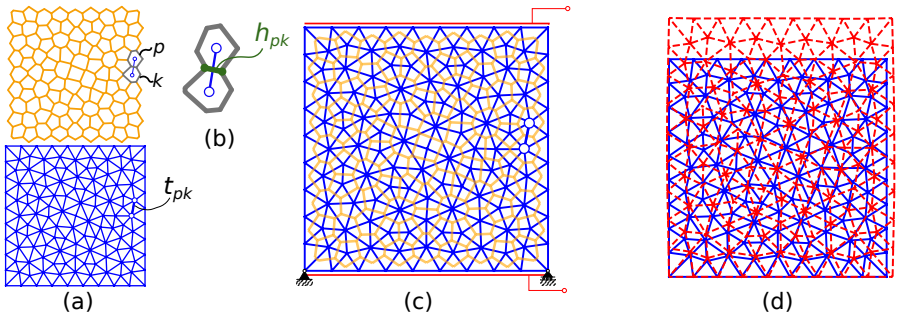

Figure 2: The lattice model represents truss network of bars t_{pk} holding together particles p and k (a). A zoom on particles p and k (b) is showing characteristic hight of the cross-section h_{pk}. The test case (c) is related to a lattice (100×100 mm^2) electroded on the top and bottom surfaces. Undeformed and deformed shapes (d) of the lattice with a scale factor of 1e5.

uniaxial stress state.
This context greatly simplifies the linear piezoelectric constitutive equations (6) reducing to two equations featuring only scalars, nemaely $\sigma = C\ \varepsilon - e\ E$, $D = e\ \varepsilon + \epsilon\ E$. That is, for piezoelectric truss the state is defined by four-tuple (ϵ, σ, E, D) of scalars related to uniaxial components of the given tensors and vectors, while the material parameters reduce to Young's modulus (C), dielectric permittivity (ϵ) and a piezoelectric constant (e) handling the coupling.

Piezoelectric material database A prerequisite for the model-free approach is the existence of the material database. As mentioned in the Introduction material data can be obtained either through instrumented or virtual experiments. For the former we acknowledge the recent effort related to so-called data driven identification (DDI) which permits us to identify the stresses directly from the full-field measurement ([11, 13, 12]). The extension of DDI to the problem at hands, that is, to the multiphysics case, will undoubtedly be the subject of future research. Some of the techniques for the surface electric potential/field measurement can be found in [32]. In this context other fields apart from stress need to be identified, in the presented piezoelectric case this is the electrical displacement vector.
The lattice model at hands boils down to one-dimensional (1D) bar problem and permits to easily deduce an analytical solution with the help of the reduced constitutive relations. Regardless of the simplicity of this 1D piezoelectric model we note that it still describes a full volume coupling. The 1D truss problem is spanning a four-dimensional phase space ($Z = \mathbb{R}^{2d_M} \times \mathbb{R}^{2d_E}$ and $d_E = d_M = 1$) related to strain, electric field, electric displacement and stress. In this rather simple context, the four-dimensional phase space resulting from the 1D problem, we can manufacture data using full factorial phase space sampling. That is, synthetic data is obtained using as two independent variables: strain and electrical

field, which are varied such that $\varepsilon_{min} \leq \varepsilon \leq \varepsilon_{max}$ and $E_{min} \leq E \leq E_{max}$. The stress σ and electrical displacement D are then obtained following the piezoelectric constitutive law (6) in reduced scalar form, and the paramters which are choosen to be $C = 54$ GPa, $\epsilon = 1.638 \cdot 10^{-8}$ N/V^2, $e = 12.96$e-3 N/V mm. Manufactured data for the simplest possible configuration are defined in four-dimensional phase space, as shown on the Fig. 3 (left). Equally this data created with the given limits in terms of ε and E can be represented as the shaded regions in the four planes$(\sigma - \varepsilon, \sigma - E, D - \varepsilon, D - E)$ shown on the Fig. 3 (right). Three different databases are generated featuring $N_m = 10^2$, 10^4 and 10^6 data

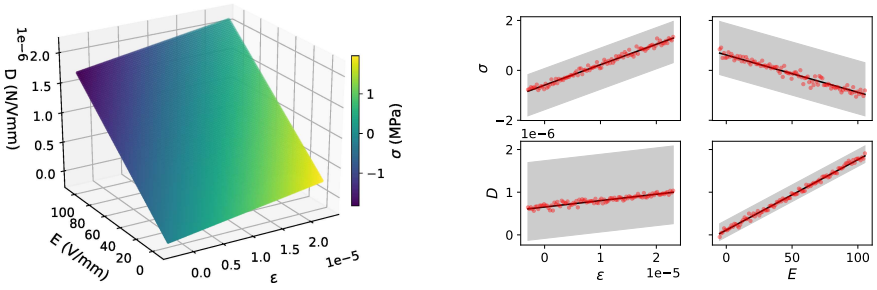

Figure 3: Manufactured data (left) for the truss problem are defined in four-dimensional phase space. In the three-dimensional plot the stress is given with the colorbar. The same database shown in the four planes$(\sigma-\varepsilon, \sigma-E, D-\varepsilon, D-E)$. The material data points fall in the shaded regions (right). Noisy data is schematically shown in the projected planes for one fixed electrical field, on the two left subplots, and for one fixed strain shown on the two right subplots.

points. More precisely, we take 10, 100 and 1000 equally spaced points for both vectors $\varepsilon_{min} \leq \varepsilon \leq \varepsilon_{max}$ and $E_{min} \leq E \leq E_{max}$ creating a regular grid. This synthetic data is used in sequel to test the convergence and performance of the proposed approach. Moreover, we will add on top of the previously generated datasets the Gaussian noise. To that end, we use a normal distribution with zero mean and standard deviation computed as the percentage p of the range

$$std_X = \frac{p}{100} \ (max(X) - min(X)) \tag{23}$$

for $p = [0.5, 1, 2, 5]$, and X being σ and D. A noisy dataset is depicted on the Fig. 3 (right) which shows the variation of stress and electrical displacement with: respect to strain for one fixed electrical field, on the two left subplots; and with respect to electrical field for one fixed strain shown on the two right subplots. The same variations without noise are depicted with black lines, resulting from the linear coupled constitutive law.

Numerical example The superposition of the deformed and undeformed shapes of the lattice is depicted on the Fig. 2 (d). We note that the relative

displacement error between the reference FE solution and our DD approach using the previously created database is less than 0.2% resulting in the virtually coincident deformed shapes. We note in passing that the distribution of the electric potential (not shown here) within the lattice also corresponds perfectly to the reference solution, totaling to the relative error less than 0.08%.
We proceed further with the convergence study. It should be noted that each cohesive element in the lattice model is naturally discretized with one single FE, and no mesh convergence analysis is necessary. We will pass on the standard convergence study in the frame of DDA related to the quality of the database. To that end we compute the global distance between computed electro-mechanical states and associated (paired) material states of the lattice as $d = \sum_i^{N_i} w_i d_i$.

For this first convergence study depicted in the Fig. 4 the exact material parameters (namely $C = 54$ GPa, $\epsilon = 16.38\ 10^{-9}$ N/V^2) are used in the DDA solver to assemble the operators $\mathbf{K}^M$ and $\mathbf{K}^E$. The evolution of the distance d with respect to the number of iterations of the DDA solver is given on Fig. 4 (left) for different database sizes, featuring $N_m = 10^2$, 10^4 and 10^6 data points. These results show a good convergence, that is, the decay of the distance d with increasing number of iterations, and significant improvement in the distance is visible for the databases comprising more data points (in the manner described above), with the price of some more iterations (namely 13, 20 and 22, respectfully for the three databases). These results are following the observations from the standard DDA, see for instance [2]. On the Fig. 4 (left) the convergence curves are overlapped for the three databases without (markers) and with noise (no markers), here with the noise $p = 1$ (see (23)). We observe that the noise seems to impact more the database with fine sampling (10^6) than the one with the coarse sampling (10^2). More specifically, the analysis of the impact of noise in a multiphysics data-driven approach would deserve more analysis. Indeed, one could define a length D associated with the uncertainty of the data. This length could be used to clean the database in a relevant way, to avoid unnecessary over-calculations. Next, we study the influence of the noise on the convergence using the database comprising 10^4 points. As expected increasing the noise level proportionally on stress σ and electric displacement D, curves labeled as 'equal' on the Fig. 4 (right), deteriorates the convergence in terms of converged distance, convergence speed and number of iterations till convergence. Note that the convergence curves (without markers) for noisy databases represent in fact the mean of five runs with random perturbations as explained above. For the visibility purpose, the spread related to five runs is depicted with the shaded band only for one curve labeled 'equal 1' on the Fig. 4 (right). In addition to equal percentage of perturbation for mechanical (M) and electrical (E) part, the convergence is plotted for the databases where either (M) or (E) parts are perturbed, corresponding to curves labeled 'mix'. From this analysis we can conclude, as visible from the Fig. 4 (right), perturbing only (M) - corresponding to curve labeled 'mix 1,0' with respect to perturbing only (E) - corresponding to curve labeled 'mix 0,1', doesn't change so much the distance at convergence. It impacts mainly the number of iteration till convergence.

On top of the (standard DDA) convergence analysis, we examine the influ-

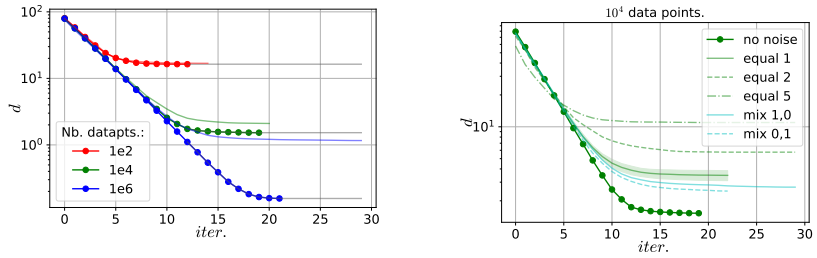

Figure 4: The convergence of the DDA solver in terms of the distance between electro-mechanical and material states d. On the left subplot the convergence is presented for different database sizes without noise (curves with markers) and for noise $p = 1$. On the right subplot the influence of the noise level is presented on the database featuring 10^4 points. For the noisy database analysis weighting parameters are taken to be $C = C_{ex}$, $\epsilon = \epsilon_{ex}$, and $\alpha = 0.5$.

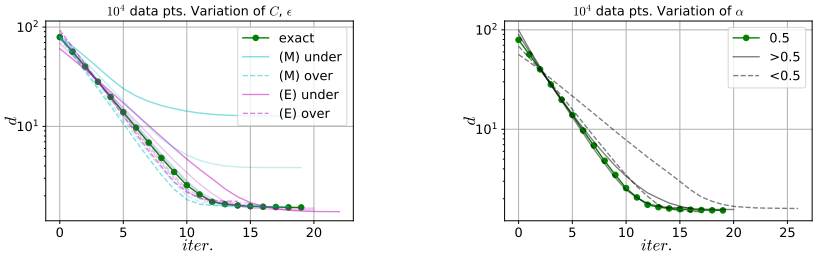

Figure 5: The convergence of the DDA solver in terms of the distance between electro-mechanical and material states d given for different weighting: (left) in terms of quasi-material parameters for (M) C and for (E) ϵ, and (right) in terms of α. In this study no noise is taken into account.

ence of parameters appearing in the norm (14). Therefore, we vary the weighting parameters C, ϵ (used in the construction of the operators $\mathbf{K}^M, \mathbf{K}^E$ and to weight σ and ε for (M) and D and E for (E)) and α (which weights mechanical end electrical terms in (14)) as follows. The parameters C and ϵ are taken to be $(\cdot)(-50, -30, -10, 10, 30, 50)\%$ of the exact values, that is $(\cdot)$ stands for $C = 54$ GPa, $\epsilon = 16.38\ 10^{-9}$ N/V[25]. The parameter α is taken to be 0.2, 0.4 to give more importance to (E) part, and 0.6 and 0.8 to give more importance to (M) part.

For the former, the quasi-material parameters variation, we noticed that for the smaller variations up to $\pm 30\%$ the influence on the convergence is virtually

[5]Even though the parameters C and ϵ represent numerical constants rather than real material parameters, they are still based on the real physical parameters. Thus, we present here the results where those numerical parameters are under/over estimated within max 50% error which is unlikely to happen in practice.

imperceptible. The exception is for highly underestimating the parameter C (DDA equivalent of the Young's modulus) as shown on the Fig. 5 (left). For the latter, the weighting parameter α, we do not notice significant effect on the convergence in the studied range. These results show finally an unimportant influence of weighting parameters on the convergence of the DDA solver in the coupled electro-mechanical context.

4.2 Piezoelectric DDA for Plane Stress

We move on with the example considering a more general case of linear piezoelectricity in the limit of plane stress. In this context, the major change with respect to previous example is related to the much higher dimensionality of the phase space. That is, each point describing either material or electro-mechanical state $\mathbf{z} = (\boldsymbol{\sigma}, \boldsymbol{\varepsilon}; \mathbf{E}, \mathbf{D})$, now lives in the 10-dimensional space $Z = \mathbb{R}^{2d_M} \times \mathbb{R}^{2d_E}$ with $d_M = 3$ for $\boldsymbol{\sigma}, \boldsymbol{\varepsilon}$ and $d_E = 2$ for $\mathbf{E}$, $\mathbf{D}$.

Piezoelectric material database Higher dimensionality of the phase space motivates somewhat different approach to manufacture material database. Contrary to the truss case from the previous example where the synthetic data is generated in a naive way in the manner of the full factorial design of experiment, here the manufactured data for the material database are obtained by performing a series of virtual tests. In the truss example, we used a full factorial design using an equidistant meshgrid whose step decreases in each dimension increased the total number of points in the database. In this manner the database was truly enriched by increasing the number of points. In this section, we propose to build the database in a different way than the previous example. We investigate the possibility to build the database from the set of simulations which are performed in the offline phase. There is no indication that increasing the number of data points with the offline simulations will lead to the database with better sampling of the material response. Offline tests are performed by running FE simulations on the 2-dimensional sample modeling a piezoelectric plate polarized in horizontal direction (this assumption is held throughout the example) featuring three holes, see Fig. 6. This particular geometry with holes is chosen merely to ensure sufficiently heterogeneous distribution of the electro-mechanical fields. The plate is discretized with 1525 piezoelectric[6], quadrilateral, plane stress elements, so-called CPS4E [33] with four integration points. The material behaviour chosen for the synthetic data creation is following the linear piezoelectric constitutive relations (6) with the parameters chosen for PZT: mechanical $E = 54$ GPa, $\nu = 0.41$, dielectric $\epsilon = 1.63 \cdot 10^{-8}$ F/m, and coupling $e_{111} = e_{122} = -9.91$ Cb/m^2 and $e_{212} = 30.24$ Cb/m^2. For simplicity we assumed here that the material behaviour is isotropic.
A synthetic data set is generated by applying different 'loading conditions' to the plate, see Fig. 7 (a) and collecting the calculated states in the integration

[6] As mentioned, the standard FE solution of the coupled problem requires a special FE formulation with added degrees of freedom.

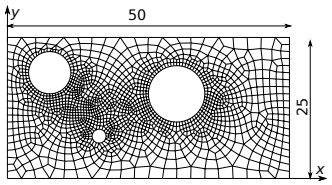

Figure 6: Piezoelectric plate polarized in $x-$ direction featuring three holes used to run virtual tests and manufacture the material database used in second example. The mesh is composed of 1525 piezoelectric, plane stress finite elements. The size of the plate is given in mm.

points. The loading cases used for the material database creation consider various positions of the electrodes placed on left, right, top and bottom surfaces, schematically shown in red on Fig. 7 (a). An example of the calculated states is shown on the Fig. 7 (b) showing the normal component of the stress and electrical displacement (*i.e.* el. flux) in vertical direction. Contour plots on the Fig. 7 (b) are related to the so called 'shear bender', a piezoelectric actuator working in the shear mode. The coupling parameter e_{212} is mostly governing the deformation mode of the chosen actuator with the polarization in the horizontal direction and the electrodes being placed on the upper and lower surfaces generating, more or less, vertical electrical field.

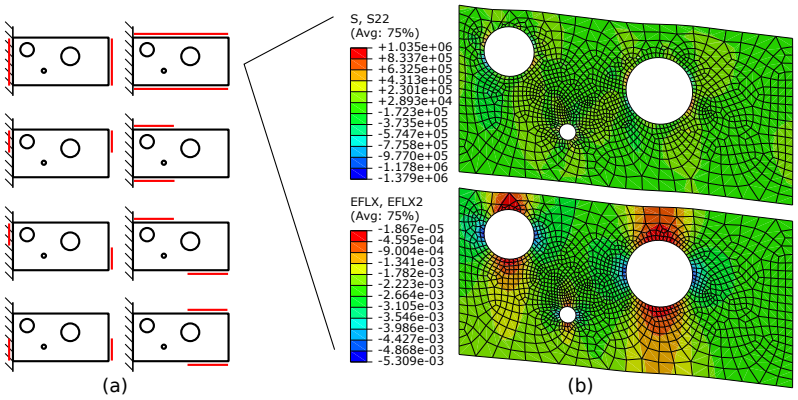

Figure 7: The loading cases (a) varied for the material database creation. These loading cases consider various positions of the electrodes placed on the left, right, top and bottom surfaces, shown in red. The distributions (b) of the normal stress in vertical direction (σ_{yy}, top) and electrical displacement (D_y, bottom) plotted on the contour of the deformed piezoelectric plate for the fully electroded top and bottom surfaces. A deformed shape of the 'shear bender' is clearly visible in spite of the heterogeneity related to the holes.

Clearly, this choice is less naive than the one used for the previous (lattice)

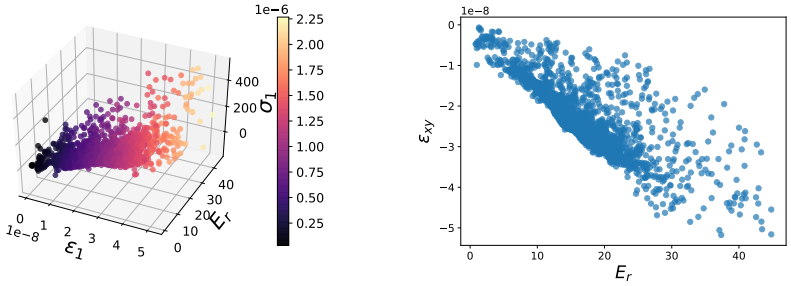

Figure 8: Representation of the 2D, plane stress electro-mechanical database for one choice of boundary conditions: in the space of principal deformation, resultant electrical field, maximal principal stress, resultant electrical displacement given with the color of the points (left); and in the input-output space (right) for the shear bender actuator, that is, E_r vs. shear deformation ε_{xy}.

example resulting in the database depicted in the left subplot of the Fig. 8. We note, however, that our virtual experiments result in the partial coverage of the electro-mechanical phase space and, more importantly, it generates significant overlap of the data points. Similarly as for the lattice example (Fig. 3 (left)), on the Fig. 8 (left) the representation of the electro-mechanical database for plane stress case (here points in 10-dimensional space) and one choice of boundary conditions is given in terms of maximal principal deformation ε_1, resultant (norm) electrical field E_r and maximal principal stress σ_1 given on the three axes. The resultant electrical displacement is given with the color of the points and the associated colorbar. Evidently, in this synthetic database we don't have states covering each deformation-electric field pair (which would lead in 10-dimensional space to huge database), but the heterogeneity of the sample provides a sufficient spread of the data points. This can be seen also on the Fig. 8 (right) for the same database which is expressed in the input-output space for the 'shear bender actuator', that is, electrical field E_r vs. shear deformation ε_{xy}. The entire material database is created by stacking the results obtained from the simulations with varying boundary conditions.

Numerical examples With the material database in hands, we proceed with two numerical examples where we are using the created material database to drive piezoelectric actuators. Namely, we consider a PZT slab polarized in the horizontal direction, electroded on the upper and lower surfaces creating a vertical electrical field, which in turn causes the in-plane shear deformation, as shown on the Fig. 9. We choose, thus, the quantity of interest for the shear bender to be the output vertical displacement, the maximal value of the output displacement is denoted as $v_{\max}$ on the Fig. 9 (b).

The first actuator shown on the Fig. 9 (b) subjected to the vertical electrical field results in homogeneous in-plane shear. In this simple case the exact

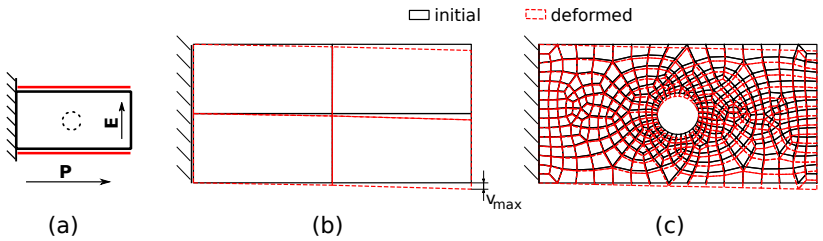

Figure 9: Boundary conditions (a) and finite element mesh (b) and (c) of the two variants of the so-called shear bender actuator made of PZT yielding a: homogeneous (b) and non-homogeneous (c) electro-mechanical states. The overall dimension of the actuators is 400x200 mm. The actuators are polarized in the horizontal direction (direction of **P** on the subplot (a)). The upper and lower surfaces are electroded causing a vertical electrical field (direction of **E** on the subplot (a)).

solution can be deduced directly from the constitutive relations and we use it to verify the proposed approach in the 2D context. To that end, a course mesh with only four finite elements is used. Since the standard shear actuator results in the homogeneous deformation we consider as the second example a PZT slab featuring a central hole, see Fig. 9 (c), which causes a somewhat heterogeneous electro-mechanical state. In what follows we extract from the overall database comprising $N_m = 50000$ points the random subsets of material states with varying size of $N_m^s = 100, 1000, 10000$ points and finally the whole generated set of 50000 points. These random samples represent different density of phase-space sampling and are used for the DDA convergence tests performed in the following analysis.

Firstly we present a comparative numerical convergence analysis of the both actuator realizations related to homogeneous and non-homogeneous cases. As before for the convergence study, we compute the global distance d between electro-mechanical states and associated (paired) material states. The evolution of d with iteration number is presented on the Fig 10 (left) for different database sizes. In the same way as for the 1D case shown above, we can see a good convergence of the local electro-mechanical-to-material states assignment, however, there is no important effect of the database size as was observed in the first example. More precisely, the whole generated database have a significant doubling of points and randomly drawing a larger subset of points (*e.g.* comprising 1000, 10000 or 50000 points) does not really improve the database quality. On the other side, the number of iterations is increased, moreover, the number of iterations is somewhat larger than in the lattice example due to the higher dimension of the phase-space. Not surprisingly, we note that the homogeneous case converges faster.

Secondly, we present the convergence of the output displacement for the shear bender with respect to the data driven solver iterations, see Fig 10 (right). The average displacement error between data driven solution (v_{DD}) and the refer-

ence, FE solution (v_{FE}) is given as

$$e_u = \|v_{\mathrm{DD}} - v_{\mathrm{FE}}\|_2 \,/\, \|v_{\mathrm{FE}}\|_2 \,. \tag{24}$$

We note from Fig 10 that the displacement error shows the same convergence behaviour. However, we note that on average we end up with about 11% of error in displacement. Surprisingly, analysis of the displacement error is not

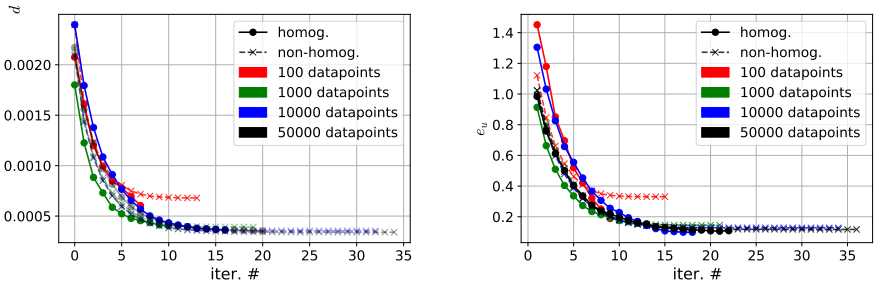

Figure 10: The convergence of the distance between electro-mechanical and material states (left) and of the average displacement error (right) for different databases.

performed in the cited references related to standard DDA. As mentioned before, in the data driven approach the displacement is merely a hidden variable within the DD solver with the energy criteria related to the chosen norm. However, the overall displacement error in our electro-mechanical case signifies that at the convergence some of the material states are still not close enough to admissible states as presented in the sequel.
The quality of a certain data (sub)set is it's ability to cover as closely as possible the phase space occupied by all the electro-mechanical states related to the chosen test case. Following this definition, we can interpret the quality of data subsets by plotting the distribution of the distances $w_i d_i$ computed in terms of the norm (14), see Fig. 11 (a). Naturally, the distances between electro-mechanical and material states are decreasing for larger datasets, which can be observed as moving the distribution to the left on the Fig. 11 (a). The spread of the presented datasets illustrates the fact that some of the electro-mechanical states are at the convergence still far from the material states in the sense of the proposed norm. In other words reducing, the dataset spread and moving it to the left results in the increase of the quality of the dataset for the actuator problem at hands. Finally, we present on the Fig. 11 (b) the distribution of the error on the contour of the non-homogeneous version of the actuator at the convergence of the data driven solver with the closest pairings found for all the integration points and the database featuring 50000 data points. On the top plot we give the contour plot of the relative error calculated as $|(u_{DD} - u_{FE})|/max(u_{FE})$. This local error is consistent with the global error shown in the convergence plot 10 (right). The lower plot on the Fig. 11 (b) presents a contour plot of the

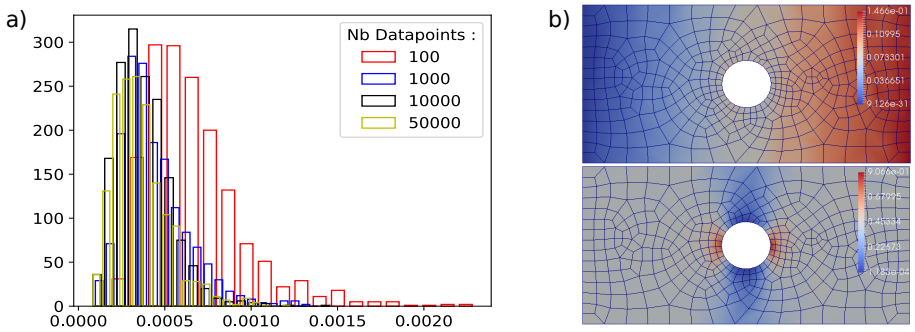

Figure 11: Distribution of the distances $w_i d_i$ for converged solution of the non-homogeneous shear bender example (a), The contour plot of the displacement and shear strain errors (b).

shear strain error between the proposed DDA and the reference FE solution, calculated analogously as the displacement error. We note that in the majority of the domain we have the local relative error close to zero. However, in the vicinity of the hole we have the error which is important even though it spreads in the limited zone.

5 Conclusion and perspectives

In this work the application of the data driven approach is proposed to adapt to the multiphysics problems. The principal idea in the data driven computational mechanics is to relax the boundary value problem and replace the explicit and empirical constitutive model in favor of the experimental data. The data driven solver then seeks to assign to each integration point of the discretized model the closest material state from the database. More precisely, the solver turns a classic solution to the constrained minimization with kinematic and equilibrium equations being the constraints. The former can be directly plugged in the optimization functional, while the latter is enforced using Lagrange multipliers.
We focus here on the active (smart) materials which owe their transducer capability to important coupling between different physical fields. In the rather general, multi-coupled context where n different fields are taken into account, the number of the coupling interactions which need to be taken into account scales with $n(n-1)/2$. Using a conventional, model-based approach one needs to have a good model that takes all the couplings into account on one hand, and the access to the custom-made finite elements featuring all the necessary degrees of freedom and their interpolation on the other. This is rarely the case in the conventional FE codes.

We have shown here that the problem being only coupled in terms of consti-

tutive equations is decoupled if there is no precise graph, say $\sigma(\varepsilon, E), D(\varepsilon, E)$. That is, the proposed application of DDA to coupled problems turns the coupled problem to uncoupled one and the coupling is completely encoded in the material database. The proposed application of the DDA to coupled problems is related mostly to the extension of the phase space and the related norm. We have investigated the performance of the data-driven solver using two particular examples of application, namely, lattice model created from planar, piezoelectric truss network and of finite element discretized linear piezoelectric solids. In both of these examples the key interaction property is due to electro-mechanical coupling. Thus, the equilibrium constraints are related to both mechanical equilibrium and Gauss law. Both of these constraints are plugged in the functional L by means of Lagrange multipliers. The stationarity equations correspond to the solution of four linear equilibrium problems which are followed by the nearest neighbour search in the phase space. Numerical tests show that the distance based data-driven solver possesses good convergence properties with respect to the database density. A prerequisite for the DD approach is the existence of the material database and herein a synthetic database is created for both problems. In the performed numerical tests we did not observe significant influence of the 'material' nor weighting parameters defined in the norm.

Although the proposed application of the DDA has been formulated in the context of electro-mechanical solids and quasistatic problems, we believe that its scope could be much larger. That is, it can be directly extrapolated to the multiphysics problems considering n coupled fields as in [16]. To facilitate the database creation (besides virtual experiments), an extension of data driven identification for the multiphysics problem should be considered. In the multiphysics case the dimensionality of the material phase space becomes even more important than in the 'monophysics DDA' case. Thus, different clustering (*e.g.* $k-$means, [34]) methods should be tested for the nearest neighbour search speed-up. Finally, imposing the non-zero Dirichlet boundary conditions (displacement, electric potential, ...) within DDA may lead to erroneous results since the loading term has a part of the stiffness comprising numerical parameters which can be under/over estimated. This study is in progress and will be a part of the next contribution.

References

[1] Michel Grdiac, Franois Hild, and Andr Pineau. John Wiley & Sons, Ltd, 2013.

[2] T. Kirchdoerfer and M. Ortiz. Data-driven computational mechanics. *Comput. Methods Appl. Mech. Eng.*, 304:81–101, June 2016.

[3] Trenton Kirchdoerfer and Michael Ortiz. Data Driven Computing with Noisy Material Data Sets. *Comput Methods Appl Mech Eng*, 326:622–641, November 2017.

[4] T. Kirchdoerfer and M. Ortiz. Data-driven computing in dynamics: Data-driven computing in dynamics. *Int. J. Numer. Meth. Engng*, 113(11):1697–1710, March 2018.

[5] Lu Trong Khiem Nguyen and Marc-André Keip. A data-driven approach to nonlinear elasticity. *Computers & Structures*, 194:97–115, January 2018.

[6] S. Conti, S. Müller, and M. Ortiz. Data-Driven Problems in Elasticity. *Arch Rational Mech Anal*, 229(1):79–123, July 2018.

[7] R. Eggersmann, T. Kirchdoerfer, S. Reese, L. Stainier, and M. Ortiz. Model-Free Data-Driven inelasticity. *Comput Methods Appl Mech Eng*, 350:81–99, June 2019.

[8] P. Carrara, L. De Lorenzis, L. Stainier, and M. Ortiz. Data-driven fracture mechanics. *Comput Methods Appl Mech Eng*, 372:113390, December 2020.

[9] Rui Xu, Jie Yang, Wei Yan, Qun Huang, Gaetano Giunta, Salim Belouettar, Hamid Zahrouni, Tarak Ben Zineb, and Heng Hu. Data-driven multiscale finite element method: From concurrence to separation. *Comput Methods Appl Mech Eng*, 363:112893, May 2020.

[10] K. Karapiperis, L. Stainier, M. Ortiz, and J.E. Andrade. Data-Driven multiscale modeling in mechanics. *Journal of the Mechanics and Physics of Solids*, 147:104239, February 2021.

[11] Adrien Leygue, Rian Seghir, Julien Réthoré, Michel Coret, Erwan Verron, and Laurent Stainier. Non-parametric material state field extraction from full field measurements. *Comput Mech*, 64(2):501–509, August 2019.

[12] Marie Dalmat, Michel Coret, Adrien Leygue, and Erwan Verron. Measuring stress field without constitutive equation. *Mechanics of Materials*, 136:103087, 2019.

[13] Laurent Stainier, Adrien Leygue, and Michael Ortiz. Model-free data-driven methods in mechanics: Material data identification and solvers. *Comput Mech*, 64(2):381–393, August 2019.

[14] Susmita Kamila. Introduction, classification and applications of smart materials: An overview. *Am. J. Appl. Sci.*, page 5, 2013.

[15] R.C. Smith, Society for Industrial, and Applied Mathematics. *Smart Material Systems: Model Developments*. Frontiers in Applied Mathematics. Society for Industrial and Applied Mathematics, 2005.

[16] Jörg Schröder, Matthias Labusch, and Marc-André Keip. Algorithmic two-scale transition for magneto-electro-mechanically coupled problems. *Comput Methods Appl Mech Eng*, 302:253–280, April 2016.

[17] José L. Pérez-Aparicio, Roberto Palma, and Robert L. Taylor. Multiphysics and Thermodynamic Formulations for Equilibrium and Non-equilibrium Interactions: Non-linear Finite Elements Applied to Multi-coupled Active Materials. *Arch Computat Methods Eng*, 23(3):535–583, September 2016.

[18] A. K. Soh and J.X. Liu. On the Constitutive Equations of Magnetoelectroelastic Solids. *J. Intell. Mater. Syst. Struct.*, 16(7-8):597–602, July 2005.

[19] R. Zabihyan, J. Mergheim, J.P. Pelteret, B. Brands, and P. Steinmann. FE2 simulations of magnetorheological elastomers: Influence of microscopic boundary conditions, microstructures and free space on the macroscopic responses of MREs. *Int. J. Numer. Meth. Engng*, 193-194:338–356, June 2020.

[20] Jiashi Yang. *An Introduction to the Theory of Piezoelectricity*. Advances in Mechanics and Mathematics. Springer US, 2005.

[21] C. Niezrecki, D. Brei, S. Balakrishnan, and A. Moskalik. Piezoelectric Actuation: State of the Art. *The Shock and Vibration Digest*, 33(4):269–280, July 2001.

[22] Henno Allik and Thomas J. R. Hughes. Finite element method for piezoelectric vibration. *Int. J. Numer. Meth. Engng*, 2(2):151–157, April 1970.

[23] Paolo Gaudenzi and Klaus-Jurgen Bathe. An iterative finite element procedure for the analysis of piezoelectric continua. *J. Intell. Mater. Syst. Struct.*, 6(2):266–273, 1995.

[24] A Benjeddou. Advances in piezoelectric finite element modeling of adaptive structural elements: A survey. *Comput Struct*, page 17, 2000.

[25] A. Butz, S. Klinkel, and W. Wagner. A geometrically and materially nonlinear piezoelectric three-dimensional-beam finite element formulation including warping effects. *Int. J. Numer. Meth. Engng*, 76(5):601–635, October 2008.

[26] Philippe Vidal, Michele D'Ottavio, Mehdi Ben Thaïer, and Olivier Polit. An Efficient Finite Shell Element for the Static Response of Piezoelectric Laminates. *Journal of Intelligent Material Systems and Structures*, 22(7):671–690, May 2011.

[27] Mickaël Duval, Jean-Charles Passieux, Michel Salaün, and Stéphane Guinard. Non-intrusive coupling: recent advances and scalable nonlinear domain decomposition. *Archives of Computational Methods in Engineering*, 23(1):17–38, 2016.

[28] Martin Ostoja-Starzewski. Lattice models in micromechanics. *Appl. Mech. Rev.*, 55(1):35–60, January 2002.

[29] N. Benkemoun, A. Ibrahimbegovic, and J.-B. Colliat. Anisotropic constitutive model of plasticity capable of accounting for details of meso-structure of two-phase composite material. *Computers & Structures*, 90-91:153–162, January 2012.

[30] M. Nikolić, E. Karavelić, A. Ibrahimbegovic, and P. Miščević. Lattice Element Models and Their Peculiarities. *Archives of Computational Methods in Engineering*, 25(3):753–784, July 2018.

[31] J.E. Bolander and S. Saito. Fracture analyses using spring networks with random geometry. *Engineering Fracture Mechanics*, 61(5-6):569–591, November 1998.

[32] P. Llovera, Ph. Molini, A. Soria, and A. Quijano. Measurements of electrostatic potentials and electric fields in some industrial applications: Basic principles. *Journal of Electrostatics*, 67(2):457–461, 2009. 11th International Conference on Electrostatics.

[33] Michael Smith. *ABAQUS/Standard User's Manual, Version 6.9*. Dassault Systèmes Simulia Corp, United States, 2009.

[34] Robert Eggersmann, Laurent Stainier, Michael Ortiz, and Stefanie Reese. Efficient data structures for model-free data-driven computational mechanics. *Computer Methods in Applied Mechanics and Engineering*, 382:113855, August 2021.